A Device for Reducing the Resistance of Transom Stern Hulls

(Ny teknik att reducera motståndet hos skrov med nedsänkt akterspegel)

Arash Eslamdoost, Mechanics and Maritime Sciences,
Chalmers University of Technology
Lars Larsson, Mechanics and Maritime Sciences,
Chalmers University of Technology
Matz Brown, SSPA Sweden AB

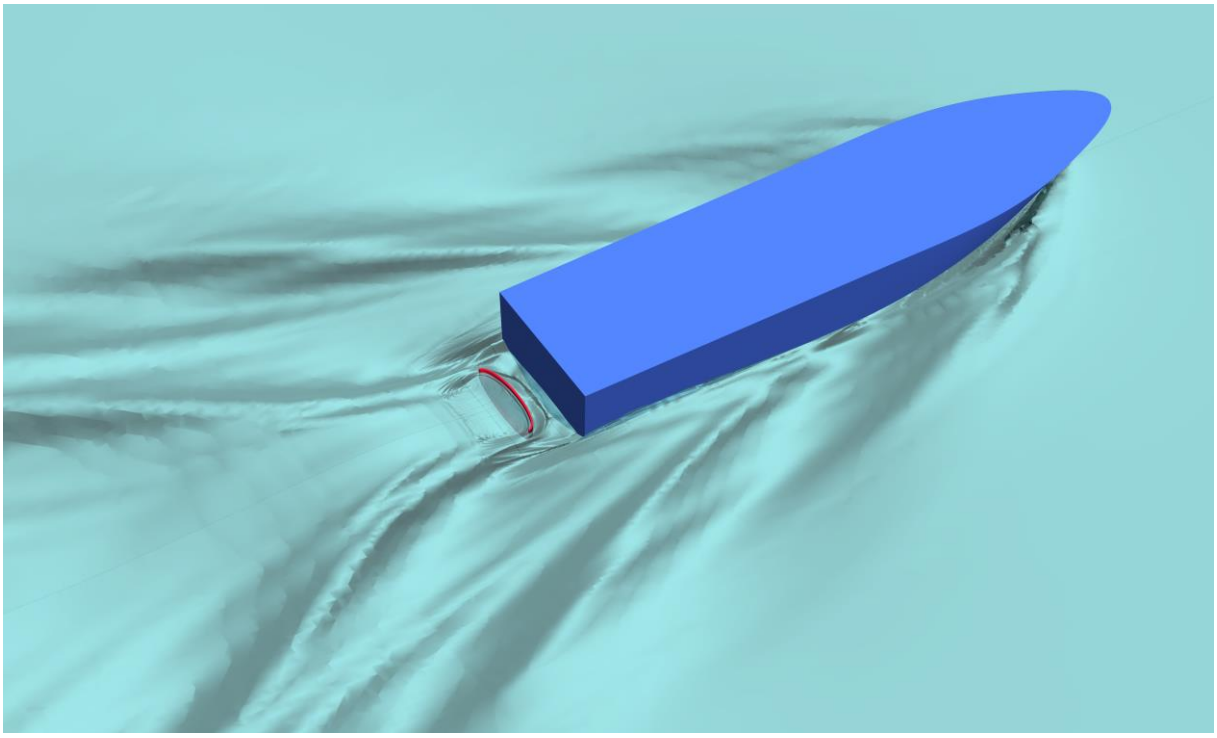

Trafikverket FUD 6482, 2018

TABLE OF CONTENTS

Abstract

A novel idea to reduce the resistance of a transom stern hull in displacement and semi-planing modes is investigated. By placing a spoon-shaped device in the recirculating zone behind the transom the momentum of the forward moving water will be absorbed and a pushing force generated on the device. Numerical and experimental techniques are applied on a transom stern hull to optimize the shape and position of the device and to explore in detail the physics behind the gain. At a Froude number of 0.4 the maximum measured resistance reduction is 11% while the computed maximum reduction is 17%. This is for the towed case. In self propulsion with one propeller the measured power reduction is 15%. Unfortunately, the power cannot be computed with the applied propeller model, but the reduction in thrust using the device is 12%. Larger gains are possible at smaller Froude numbers, while the effect is reduced when the Froude number is higher. By splitting the thrust on two propellers even larger gains are possible. However, the device is not suitable for waterjet propulsion. All results in this report are for model scale. Larger gains are expected at full scale.

1 Introduction

For boats and ships running at speeds in the semiplaning and planing speed ranges transom sterns are the only viable option. Cruiser type sterns cannot be used, since the hull lines would then be strongly curved on the aft body, creating a large suction force, increasing both resistance and trim by the stern.

A model of a planing transom stern hull operating at two different speeds is shown in Figure 1. In the lower speed range, the transom is wet but there is a critical speed for transom stern hulls, where the water surface leaves the transom tangent to the bottom and thereafter the transom becomes dry. Before this critical speed, the water is dragged along with the hull in a massively separated zone behind the transom. This is basically an unwanted flow feature and is considered as a source of loss which increases the hull resistance.

Figure 1.The flow pattern around a planing transom stern hull at two different speeds. The hull transom is wet below the critical speed (left) and it becomes dry above the critical speed (right).

Figure 2 shows a typical example of a hull running in the interesting speed range. This is a passenger boat operating in the Gothenburg archipelago. Many boats of this kind are found around the Swedish (and Norwegian!) coast line. Other typical examples are fishing vessels at trawling speeds and naval craft.

Figure 2. Älv-snabben 3 with a recirculating water region behind its transom (Photo: Arash Eslamdoost).

In the present project, we investigate a new technique to reduce the fuel consumption of ships operating around transom clearance speed. The basic idea is to make use of the recirculating water energy and the breaking rooster tail wave behind the hull at speeds below the critical one, where the water clears the transom. This idea has a patent pending both in Sweden and Europe and no similar technique is known by the patent authorities.

In order to reduce the energy loss in the recirculating water region behind the hull a device is placed inside this region to stop the water from moving forward (in the direction of hull movement). The device absorbs the momentum of the forward flowing water and pushes the hull forward. The overall result is a reduced total resistance.

Figure 3. Placing of the Transom Pushing Device (TPD) in the computations (left) and the experiments (right)

Figure 3 shows a configuration which was used in preliminary Computational Fluid Dynamics (CFD) simulations and experiments. Inserting the Transom Pushing Device (TPD) in the dead-water region splits the bare hull recirculating zone into two separate regions (Figure 4). The shape and the horizontal and vertical positions of the device influences the flow and thus the forward pushing force. The preliminary computations and experiments indicated a resistance reduction of 4-9%.

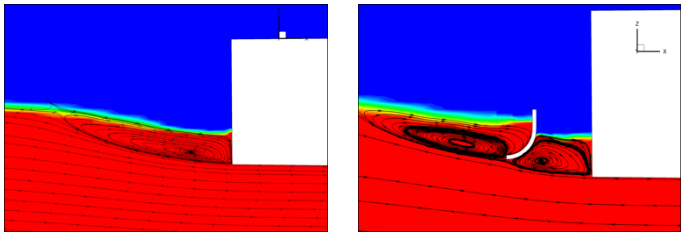
Figure 4. Recirculating water region on the symmetry plane behind the bare hull transom (left) and with the Transom Pushing Device (TPD).

All preliminary simulations and tests were performed with a towed hull without any propulsion. Moreover, no optimisation study was carried out to find the best position of the TPD. The objective of the present work is to better understand the physics of the TPD and to optimize the position both in towing and self-propulsion mode. The investigation is carried out using both CFD and experiments (hereinafter called EFD: Experimental Fluid Dynamics).

In the following the example hull and the TPD are first introduced in Section 2. Thereafter the CFD technique is described in Section 3, followed by the EFD technique in Section 4. In Section 5 the computed and measured results are presented and finally, in Section 6, some conclusions are drawn.

2 Test case

The hull used in this study is a planing hull designed by SSPA, with the model number 3209-B. In the following, this hull is referred to as the SSPA hull. A body plan is presented in Figure 5, and the longitudinal position of the hull sections are shown in Figure 6. The aft and fore perpendiculars are the sections which are marked by the numbers 0 and 20, respectively. Draft measurements are carried out at these sections. The towing point of the hull is 95 mm below the deck level and is located at section 6 shown in Figure 6. In Table 1 the particulars of the hull are given.

Note that this hull is designed for Froude number 0.8, while the main interest in the present investigation is in the Froude number range 0.2-0.6. This means that the transom is larger than for a ship designed for this range, and that the effects investigated in this project may be somewhat exaggerated. The reason for using this hull was that the model was available and that

all initial investigations had been carried out for with this model. Quite often, hulls designed for larger speeds run at a lower speed long periods of time (naval craft, passenger ferries in the archipelago, fishing vessels, …). Then the present Froude number range is relevant.

It should be stressed that all results of this work are in model scale. Since the effects are caused by pressure changes which are (almost) scale independent, larger effects may be expected at full scale, where the fictional forces play a smaller role.

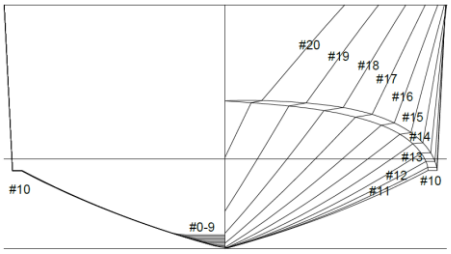

Figure 5. Body plan of test hull

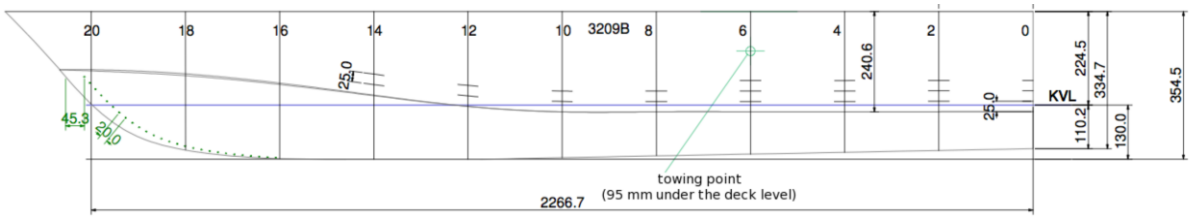

Figure 6 Contour of test hull

Table 1. Hull particulars (Note all results are at model scale)

Scale factor α [-]	7.500		
Length L_{PP} [m]	17.00	Beam B [m]	4.65
Length L_{WL} [m]	16.98	Displacement [m^3]	35
Draft forward T_F [m]	0.98	Draft aft T_A [m]	0.98

The 3D printed propeller geometry is shown in Figure 7. It has 5 blades with outer diameter of 100 mm. This propeller is not designed to operate at low speeds and thus its efficiency in the measurement speed rage is lower than its best efficiency.

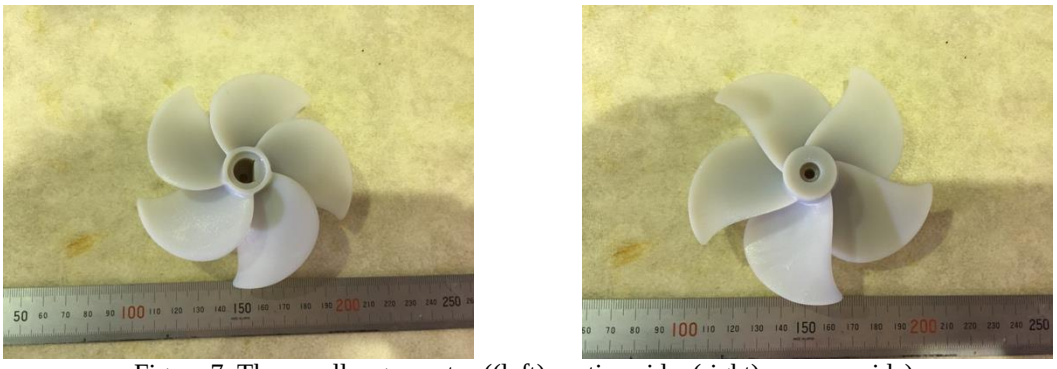
Figure 7. The ropeller goometry ((left) suction side, (right) pressure side).

The location of the propeller and the TPD are defined in Figure 8. Hull with TPD and propeller. Systematic variations of the TPD are reported in Sections 5.3 and 5.4. In CFD, the propeller is

represented as a body force disk, shown in the figure. Note that this disk is vertical! This is to enable a better alignment with the grid, and thus smaller numerical errors. However, even if the disk is vertical the body forces are directed along the imagined shaft, inclined 10 degrees relative to the bottom. Note that no shaft was present in the computations. In the experiments there was a physical shaft and the propeller was naturally at right angles to the shaft. The center of both propellers was the same, and the position is shown in the figure.

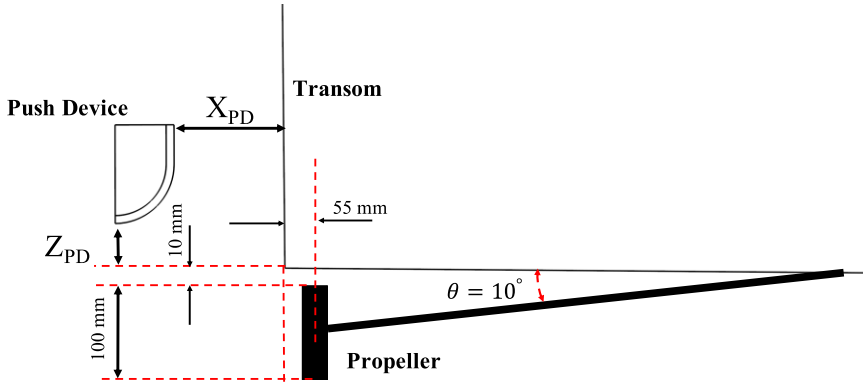

Figure 8. Hull with TPD and propeller. The definition of the TPD position is also shown as X_{PD} and Z_{PD}. The coordinate system has its origin at the transom stern edge, X is directed backwards and Z vertically upwards. The unit is mm.

A detail of the TPD mount is shown in Figure 9. The TPD (20 in the Figure 9) is attached to a vertical bar (21) along which it can slide for different vertical positions. The bar is attached to a balance (17), which in turn is attached to a horizontal U- beam (2). This beam can slide longitudinally to position the TPD at different distances from the transom. The balance measures horizontal and vertical forces.

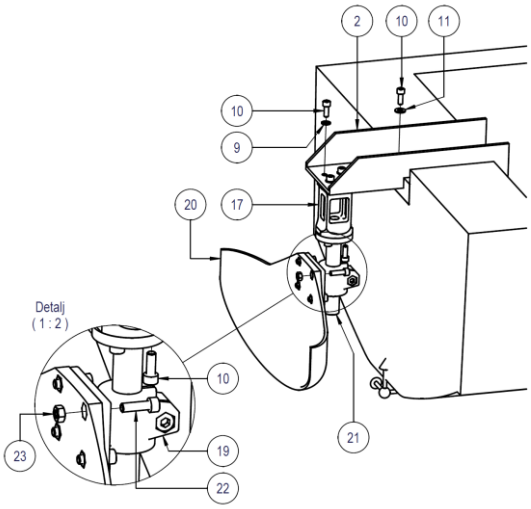

Figure 9. Details of the TPD mount

3 Numerical method

3.1 Numerical details

The numerical simulations were carried out with the code STAR-CCM+ 13.02. A Finite Volume method in combination with control volumes consisting of arbitrary polyhedrals is used in this code to solve the unsteady mass and momentum conservation equations in integral form.

An implicit unsteady time stepping method is used. This method has a wide stability range (Courant number larger than 1) and therefore allows large local time steps. The Volume of Fluid (VOF) method is used to obtain the volume fraction of the liquid, which adds one more equation to the system of equations. Convective terms in this equation are discretized using the HRIC-scheme. The free-surface interface is expected to be sharp since this equation resolves the free-surface within typically one cell. The k-ω SST turbulence model is used to compute the turbulence effects on the mean flow. Hence, two more equations need to be solved, one for the kinetic energy, k, and one for the specific dissipation rate, ω. The boundary layers are resolved down to the wall and no wall functions are used. This system of equations is solved using a segregated iterative solution method based on the SIMPLE-algorithm.

In the present project simulations are carried out both with the fixed and free sinkage and trim, as will be seen below. In order to compute the dynamic equilibrium position of the hull, the initial sinkage and trim of the hull are set to the measured values. Before starting the 2DOF (free sinkage and trim) modeling the simulations are carried out with the fixed sinkage and trim until the pressure and viscous forces exerted on the hull are stabilized. Then the hull is released to heave and pitch and the 6DOF solver starts to update the equilibrium position of the hull iteratively.

When the hull is free to move in the simulations a towing force needs to be applied to the hull at the position where the hull was towed in the towing tank. The position of the tow force is shown in Fig. 6. It was tried to keep the tow force parallel to the keel line during the resistance tests. In the computations, the magnitude of the tow force at each iteration is set equal to the resistance of the hull computed from the previous iteration.

3.2 Grid

Considering the symmetry of the flow only half of the geometry is used. Trimmed hexahedral grids and prism layers along walls are used to create the grids. Trimmed grids allow anisotropic local refinement around the hull and the free-surface. Four levels of refinement inside arbitrarily defined volumes are used for the free-surface and around the hull to capture the free-surface (Figure 10). Since the aim of this study is to investigate the transom flow, the finest refinement level is used in this region as shown in Figure 11. The prism layer grid used to resolve the boundary layer is seen below the hull in the symmetry plane.

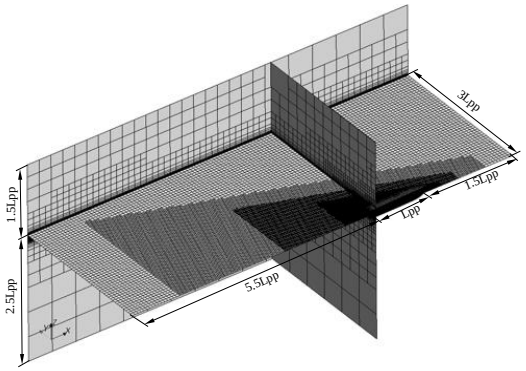

Figure 10. The structure of the mesh illustrating the refined zones. Arrows show the dimensions of the computational domain expressed in the hull Lpp.

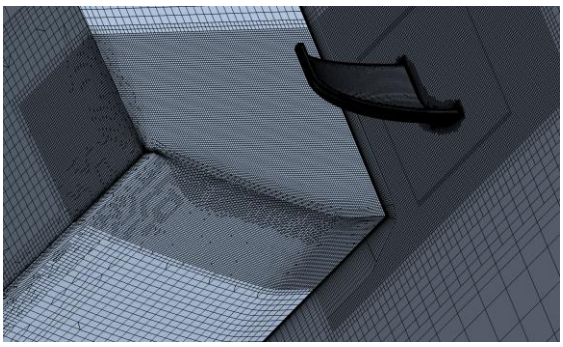

Figure 11. Closer look to the mesh around transom and TPD.

3.3 Verification

To obtain a suitable cell size, and hence total grid number, a systematic grid refinement study was carried out for Froude number 0.4 with the TPD at (X,Z) = (113, 45). See Figure 8 for a definition of the coordinate system! This is just below the critical Froude number, where the water clears the transom. Eight grids with systematically varied grid parameters were used. The number of cells in the coarsest grid was $0.944E6$ and in the finest $14.9E6$. In Figure 11 the convergence of the solution for the resistance coefficient C_T is shown. Since the grid is unstructured, the step size h_i on the horizontal axis is obtained as the inverse of the third root of the total number of cells for grid i. h_1 represents the finest grid. Table 2 shows details of the systematically refined grids.

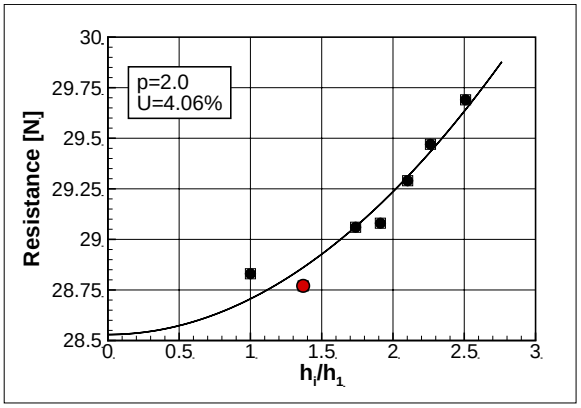

Figure 12. Convergence of the total resistance coefficient with grid refinement at $Fn = 0.4$. Hull with TPD. The red cicle indicates the grid used in this study.

Table 2. Grid refinement parameters

Refinment Ratio	Number of Cells	R_T [N]
1	1.49E+07	28.83
1.4	5.80E+06	28.77
1.8	2.84E+06	29.06
2	2.14E+06	29.08
2.2	1.60E+06	29.29
2.4	1.29E+06	29.47
2.6	9.44E+05	29.69

A formal verification based on the Least Squares Root method by Eça and Hoekstra was also carried out. This showed that a good compromise between numerical accuracy and computational effort was obtained with the second finest grid, which was selected for further computations. The number of cells for this grid is $5.8E6$ and the numerical uncertainty 4.06%. It should be noted that the verification method is for steady flows, while some unsteadiness was detected in the present computations, particularly at Froude numbers below the critical one. A certain dependence on the time step may thus be expected.

Since no wall functions are used y+ has to be quite small, around 1 at the maximum. Figure 13 shows the distribution of y+ over the wetted surface. As can be seen the values are close to 1 except in thin strips in the bow wave. Presumably this will have a negligible effect, since the regions are very small.

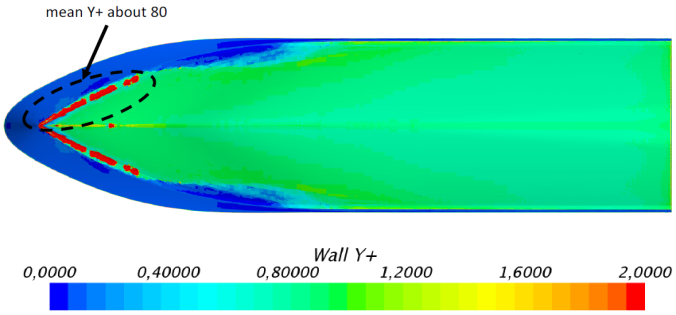

Figure 13. Distribution of y+ on the hull at $Fn = 0.4$. Hull with TPD.

3.4 Validation

Validation was done for the bare hull (BH) without TPD. Figure 14 shows the predicted and measured resistance vs. Froude number. The difference (comparison error) is shown in Figure 15. At the most interesting Froude number around 0.4 the comparison error is around 4%, while it is maximum 8 % in the range 0.35-0.60. For the lowest Froude number, the comparison error is rather large, 14%. Note that the comparison error includes both computational and measurement errors. Unfortunately, no estimate of the experimental error was available, so a formal validation cannot be made. However, we can note that the comparison error for Froude number 0.4 is about the same as the numerical uncertainty, while it is larger at the other Froude numbers.

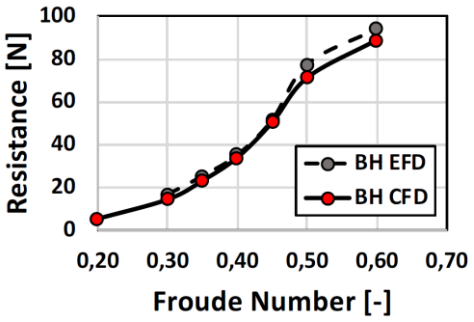

Figure 14. Measured (EFD) and computed (CFD) total resistance for the bare hull without TPD.

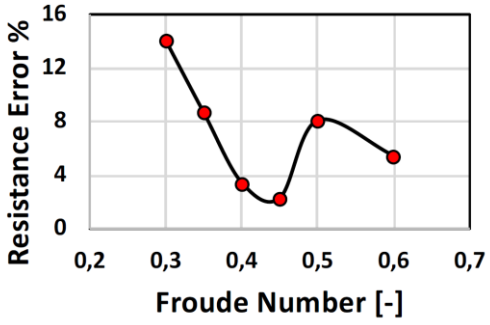

Figure 15. Comparison error in percent of measured value.

Aft draft and trim results are shown in Figure 16 and Figure 17. The correspondence between CFD and EFD is reasonably good except at the highest Froude number.

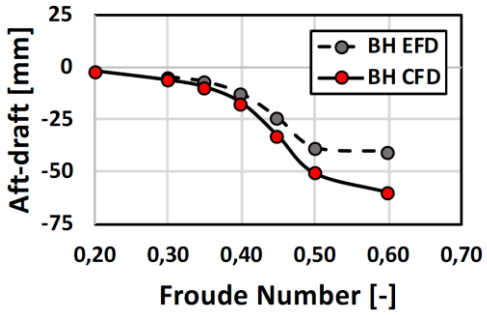

Figure 16. Measured (EFD) and computed aft draft for the bare hull without TPD

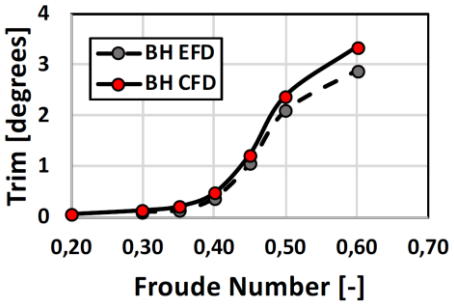

Figure 17. Measured (EFD) and computed (CFD) trim angle for the bare hull without TPD

4 Experimental technique

4.1 Test facility

The tests were performed in SSPA's towing tank, which has the following main particulars:

- Length 260 m
- Breadth 10 m
- Water depth 5 m

The towing tank is spanned by a gantry carriage from which the ship model is towed. All tests were performed in calm water.

4.2 Test arrangement

The model was ballasted to the corresponding full-scale volume displacement. The draught was verified at forward perpendicular (FP), mid ships (MS) and aft perpendicular (AP), on both sides of the model. During testing, the model was fixed axially to the carriage with a rod and an electrical transducer that measured the towing force exerted on the model. As the rod was adjusted to be parallel to the baseline, the force was measured in the horizontal direction at all tests. The model was kept on course by two trim devices, one at each perpendicular. These devices also served to prevent the model from surging, swaying and yawing while leaving it free to heave, roll and pitch.

When moving the TPD longitudinally, the center of gravity moved backwards. This was compensated by moving a ballast weight in the longitudinal direction.

The following signals were measured and registered by a computer on the carriage:

- Model speed
- Towing force
- Vertical motion at FP
- Vertical motion at AP
- Vertical force on pushing device
- Horizontal force on pushing device
- Propeller shaft torque
- Propeller RPM

Photographs of the surface wave pattern were taken by above-water cameras at the bow, stern and amidships during the tests. Video recordings of the flow were also taken in the region around the stern.

5 Results

5.1 Design of the TPD

The operational concept of TPD is to utilize the wasted energy in the recirculating water behind transom in the lower speed ranges when transom is still wet. In the initial design phase two flat plates with simple shapes where placed in the recirculating water region. These geometries are shown in Figure 18. The plates where placed at the same longitudinal distance from the transom and an optimization study was carried out for obtaining the largest resistance reduction as a function of vertical distance from the transom edge. These preliminary studies showed a resistance reduction of 2.8% for the rectangular plate and 4.6% for the triangular plate. The pressure distribution on both sides of the plates are shown in Figure 19 and Figure 20.

The high pressure on the rectangular plate for the face pointing towards transom shows that these corners penetrate the free-stream flow. This will reduce the efficiency of the flat plate and indeed was the reason for designing the triangular TPD. The lower pressure on the same face of the triangular TPD shows that trimming the lower corners of the rectangular plate works in a favorable direction and the triangular TPD does not penetrate the free-stream flow any longer. As mentioned, this modification improved the performance of TPD by about 2% in comparison to the rectangular TPD.

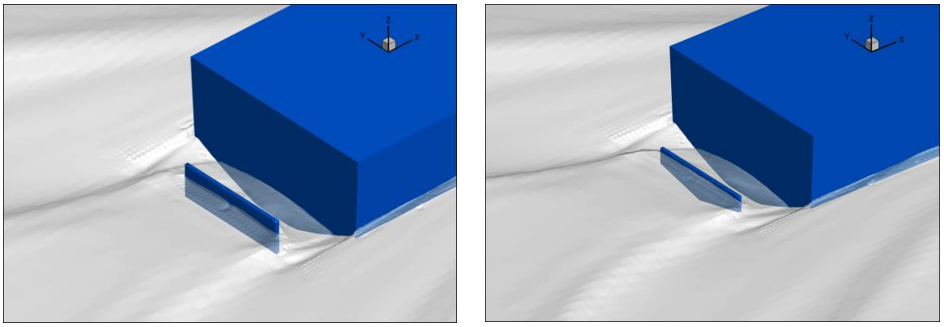

Figure 18. Application of a rectangular plate (left) and a triangular plate (right) for TPD.

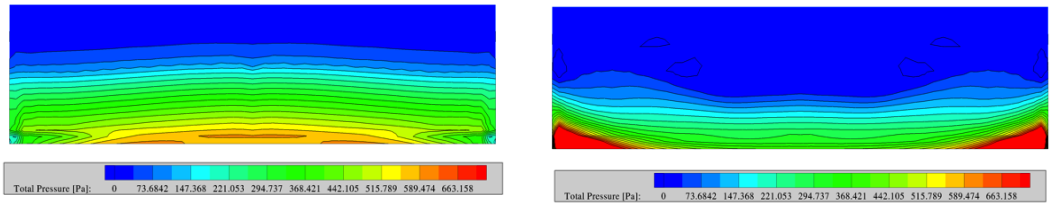

Figure 19. Pressure distribution on the rectangular TPD, the face with its normal surface vector aligned with transom's normal surface vector (left) and the face with opposite normal surface vector with respect to transom's normal surface vector (right).

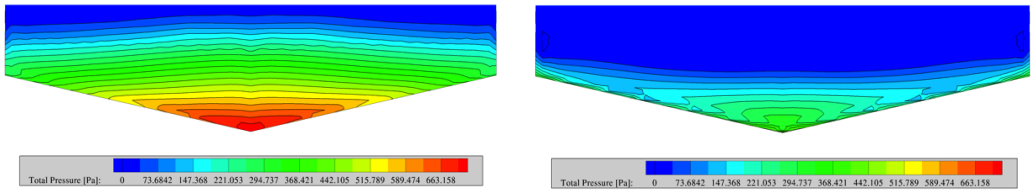

Figure 20. Pressure distribution on the triangular TPD, the face with its normal surface vector aligned with transom's normal surface vector (left) and the face with opposite normal surface vector with respect to transom's normal surface vector (right).

However, we know that the flat triangular TPD is not streamlined and its sharp edges may increase the system resistance in case it penetrates the free-stream flow. In order minimize the risk of increased resistance in the aforementioned scenario, instead of a flat plate, it would be better to have a curved surface which allows the free-stream flow to pass smother. Moreover, the TPD can cover a larger recirculating water area if its form is adapted according to the structure of the recirculating region which itself is a function of the transom shape as well as the operating speed of the hull. Figure 21 shows the streamlines behind the transom in half of the recirculating region. There are also several cross sections shown in this figure. The dark blue region shows flow in the direction opposite to the hull motion and the red color highlights the region which the flow has the same axial velocity direction as the hull. The TPD task is to take the advantage of the energy in this flow region and reduce the resistance. The cross sections marked with red can be used to design an improved TPD form which is adapted to this region. The projected area of the new design in Figure 22 is taken from one of the cross sections and its edges are curved backwards to avoid a sudden increase in resistance in case it moves out of the recirculating water zone. The new design of the TPD is shown in Figure 23. In the preliminary design stages, the new design showed a resistance reduction of 5.7% which was 1.2% better than the triangular TPD. Note that this improvement was obtained in early design phase of the project and later through a systematic variation of TPD position we managed to improve the performance (about 17% resistance reduction with the same TPD design). The study on the systematic variation of TPD position is presented in Section (5.3).

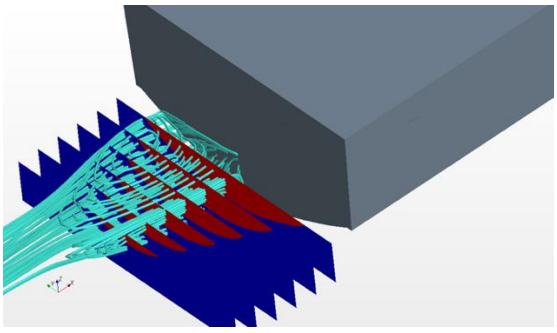

Figure 21. Streamlines in the recirculating water region as well as split of the flow based on its direction. The flow moving in the opposite direction relative to the hull motion is shown in dark blue and the flow mowing towards transom is shown in red.

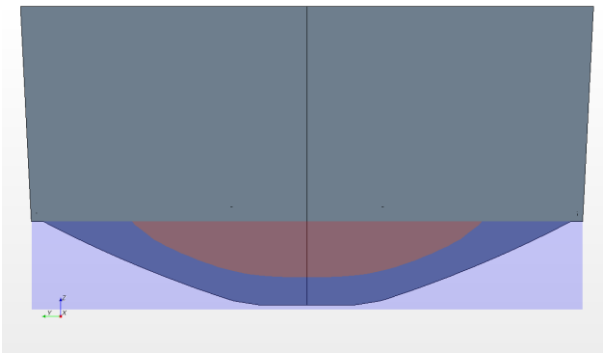

Figure 22. One of the cross sections shown in Figure 21

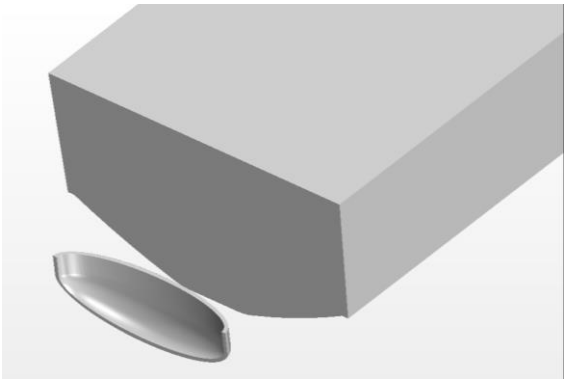

Figure 23. Wake adapted design for the TPD.

5.2 Physical understanding

The basic idea behind the TPD is to take advantage of the momentum in the forward direction found in the recirculating zone behind the transom. A device with a large resistance in this forward flowing water would create a pushing force when attached to the hull. However, preliminary calculations indicated that there may be other unexpected effects of significant importance. In this Section we will use CFD to investigate the physics of the TPD. How does it really work?

The first question is whether the effect is local, i.e. related to the local flow behind the transom, or global by changing the hull attitude (sinkage and trim). In other words: does the TPD act as a trim plane and reduce the resistance by reducing the size of the (too large) transom?

5.2.1 Global vs. local effect.

To investigate this, three cases are compared for the optimum position (see Table 5) of the TPD at (113, 25) and at Fn = 0.4, without the propeller. Apart from the bare hull without the TPD (BH) and with the TPD (BHPD) a case was run with the same sinkage and trim as BHDP, but without the TPD (BH_BHPD). In this way the effect of changes in sinkage and trim may be evaluated. The results are seen in Table 3, where the resistance contributions are split into three components: the hull excluding the transom, the transom and the TPD.

Table 3. Effect of sinkage and trim changes on resistance [N]

	BH	**BH_BHPD**	**BHPD**
Hull	42.6	41.5	41.8
Transom	-7.8	-7.5	-8.9
TPD	-	-	-4.6
Total	34.7	34.0	28.3

From the last row it appears that the total resistance changes very little due to the sinkage and trim change, from 34.7 N to 34.0 N. The effect of adding the TPD (for the same trim) is an order of magnitude larger, a change from 34.0 N to 28.3 N. It may also be seen in the table that the resistance reduction due to the changed sinkage and trim mainly comes from the hull (42.6 N changed to 41.5N), while the transom contribution changed very little (-7.8 N to -7.5N). Adding the TPD increased the transom contribution much more (from -7.5 to -8.9), while by far the largest resistance reduction is due to the force from the TPD (-4.6 N). This investigation thus confirmed the original idea that it is the force on the TPD that causes the resistance reduction *when the TPD is in its optimum position*.

One effect which was not foreseen in the original TPD idea was the increase of water level on the transom, thereby increasing its pushing force. As we have seen in Table 3, there is indeed such an effect, at least for this condition. In Figure 24 the relative importance of the TPD and the increase in transom pushing force is shown for varying *longitudinal* positions of the TPD but with the vertical position fixed to the optimum at Z=25 mm. There is also a curve for the change in hull resistance (excluding transom).

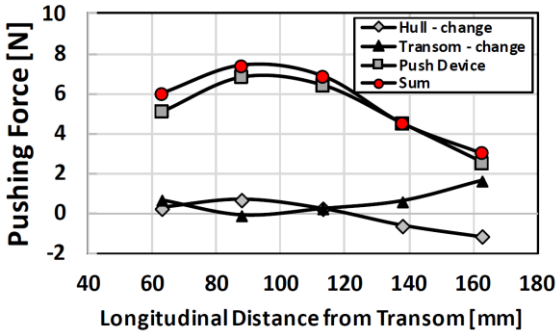

Figure 24. Contribution the pushing force from TPD, transom and hull against TPD horizontal position variations.

It is seen that the TPD is the most important contributor to the pushing force at all longitudinal positions. The transom change contribution is much smaller, but positive. For large distances the transom effect approaches the TPD effect. The hull effect is small and positive at small distances, but negative with the TPD far away from the transom.

The raise in water level at the transom for the optimum position is shown in Figure 25. For this case, the increase in wetted area on the transom is 9.6%.

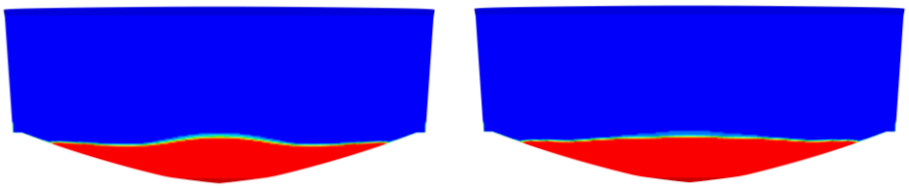

Figure 25. Wetted surface on the transom without and with TPD. Red colour; water

It may be of interest to also look at the water levels on the two sides of the TPD. These are shown for the reference case in Figure 26. The water level is much higher on the rear side as expected. This reflects the different pressures and it is the pressure difference that gives the pushing force. The pressures are presented in Figure 27, and in Figure 28 the pressure forces on the two sides are displayed as a function of the TPD position. The positive contributions to the pushing forces from the rear (concave) side are much larger than the negative contributions from the front (convex) side. This is particularly so for the optimum longitudinal position and at smaller distances to the transom. At larger distances the positive force is reduced and the negative one increased (absolute value), which means that the total TPD force is reduced considerably. Note that all this is for the optimum vertical position (Z=25mm).

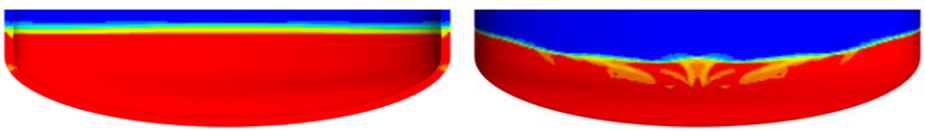

Figure 26. Wetted surface on TPD. Left: rear surface. Right: front surface

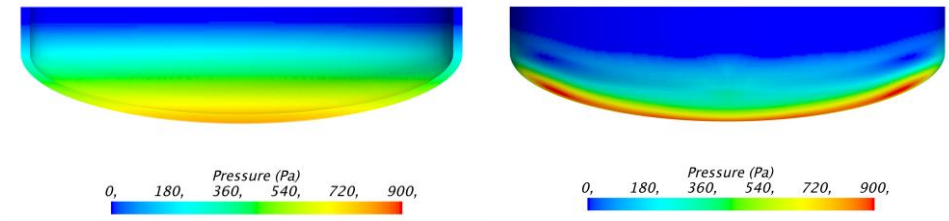

Figure 27. Pressure distribution on the TPD. Left: rear surface. Right: front surface

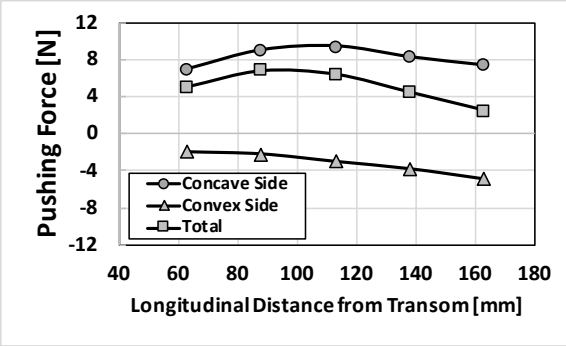

Figure 28. Contribution to the total pushing force on the TPD from the two sides

The findings above are completely changed if the vertical position of the TPD is varied. Figure 29 shows again the contributions from the TPD, the transom and the hull (excluding the transom). But now the axial position is fixed to the optimum (X = 113mm), while the vertical position is varied. Apparently the relative contributions change drastically for non-optimum vertical positions. But interestingly enough, the sum of the contributions, i.e. the total effect, is relatively constant. If the TPD is pushed down into the free stream water moving backwards, its pushing force will naturally be reduced. When it approaches the level of the transom edge the TPD will create a drag force. However the high pressure in front of the TPD in this position will raise the water level on the transom, thereby increasing its pushing effect. Also, the TPD will act as a trim plane and create a bow-down trim, which reduces the hull drag due to the too large transom.

If the TPD is lifted above the optimum position the pushing force is naturally reduced. It does not take full advantage of the recirculating flow in this position. However, even in this case there is a raise in the water level on the transom, which increases its pushing effect and partly compensates for the loss in TPD force.

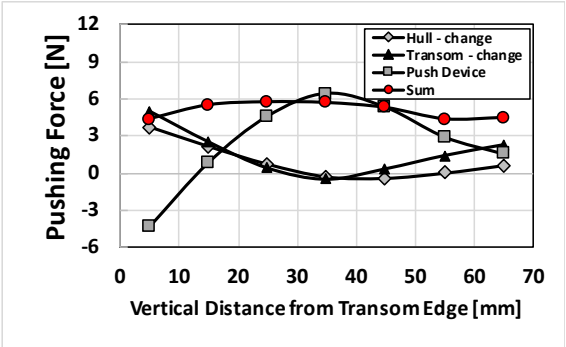

Figure 29. Contribution the pushing force from TPD, transom and hull against TPD vertical position variations.

5.2.2 TPD effect on the wave pattern

The basic idea is that the TPD shall take advantage of the forward moving water in the recirculating zone. The question is whether it also changes the transmitted wave height. Figure 30 shows the wave pattern for the optimum position at $F_n = 0.4$. It is clearly seen that there is a reduction in wave height caused by the TPD, at least close to the hull. Figure 31 shows the wave height in the symmetry plane behind the hull. Again, a reduction in wave height is seen close to the hull, but the effect seems to decay with distance from the hull.

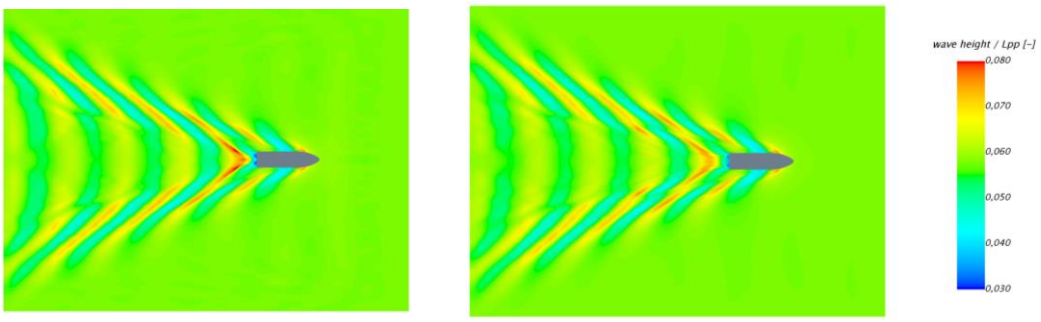

Figure 30. Wave pattern at optimum TPD positio, F_n = 0,4. Left: without TPD. Right with TPD

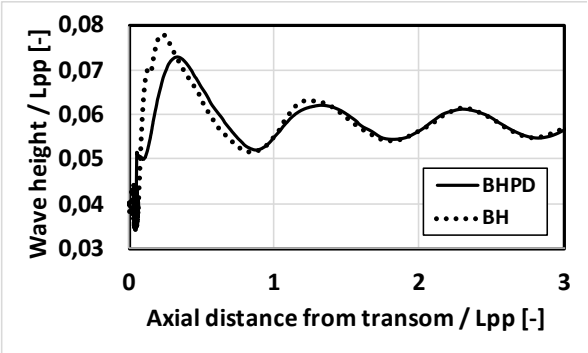

Figure 31. Wave height in the symmetry plane behind the hull. BH: without TPD. BHPD: with TPD

5.2.3 Momentum analysis

In order to further explore the effects of the TPD a momentum analysis was made for the control volume (CV) shown in Figure 24. This was done with and without the TPD. It should be stressed that such an analysis is very hard to do with large accuracy, particularly with a free surface present. Ideally the CV boundaries should be far away from the body, but in any CFD solution the numerical damping will render such results meaningless. Therefore, the boundaries are quite close to the hull.

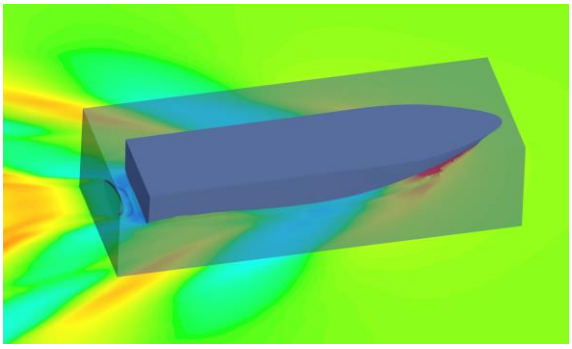

Figure 32. Control volume (CV) for the momentum analysis

Table 4. Momentum analysis for the reference case. BH: bare hull without TPD. BHPD: bare hull with TPD (here BH has the same sinkage and trim as BHPD)

Table 4. Momentum analysis

Momentum Flux [N]						
	Bottom	**In**	**Out**	**Side**	**Top**	**Sum**
BHPD	70.35	-978.98	860.21	60.53	-0.09	12.01
BH	66.36	-978.99	866.94	58.53	-0.11	12.72
Difference	3.99	0.01	-6.73	2.00	0.02	-0.71
Pressure Force [N]						
	Bottom	**In**	**Out**	**Side**	**Top**	**Sum**
BHPD	0.00	395.48	-356.48	0.00	0.00	39.00
BH	0.00	395.55	-351.85	0.00	0.00	43.70
Difference	0.00	-0.07	-4.63	0.00	0.00	-4.70

Table 4 shows the flux of longitudinal momentum out of the CV for the different sides (top) and the pressure forces acting of the sides from the exterior (bottom). Note the positive direction is backwards. As expected, there is no change due to the TPD in the flux out of the inflow and the top (in the air), while the flux has increased at the bottom and sides, and decreased in the outflow. The net sum is very small, only -0.71 N. The pressure forces are practically unchanged at all sides, except for the outflow, where the force change is -4.70 N. The pressure has thus increased behind the TPD compared to the case without the TPD.

Now, according to the momentum theorem the net flux of x-momentum out must be equal to the sum of all forces acting on the CV in the x-direction. The x-force has two components: the pressure acting on the surfaces of the CV and the force required to tow the hull, which acts on the water by the hull surface. The tow force is thus equal to the net momentum increase minus the CV surface pressure forces. For BHPD this is 12.01 – 39.00 = -26.99 N. For BH it is 12.72 - 43.70 = -30.98. These forces are lower than those obtained by direct integration of pressure and friction on the hull surface (which are 28.32 and 33.60, respectively) due to the difficulties of applying the momentum theorem mentioned above. However, we believe that the accuracy is high enough for the present qualitative analysis of the TPD gains.

From the momentum analysis there is a change in tow force by -26.99 + 30.98 = 3.99 N. We have to tow the hull with a force which is 3.99 N smaller with the TPD. As we have seen above this reduction comes mainly from the increased pressure behind the CV. There are changes in the momentum flux through the sides due to the TPD, but they more or less cancel out.

5.3 Systematic variations with and without a propeller

In figures above, the optimum position of the TPD has been used as reference and the effect of variations have been discussed, referring to this Section. Here the full matrix of variations will be presented. To obtain the optimum position of the TPD, computations with a systematic variation in position were carried out with and without the TPD for the towed hull and the self-propelled one. In Table 5 the gains with the TPD for the towed hull are presented. The gains are visualized in Figure 33. The maximum gain is obtained at the reference position (113, 25) and is 16.75%. As seen above, the gains are rather constant with X over the range for the best heights, but for the lowest and highest positions the gains drop considerably at the end points.

Table 5. Computed resistance reduction with TPD for varying positions. Bare hull.

x [mm]	63	88	113	138	163
z [mm]					
65	10.81	12.40	12.98	13.04	3.64
55	11.02	12.22	12.90	13.92	5.46
45	12.63	13.98	15.54	14.98	9.49
35	13.75	15.57	16.72	14.45	13.66
25	13.37	15.95	16.75	16.25	16.04
15	14.95	15.95	16.22	15.07	14.48
5	4.02	13.01	12.72	11.52	10.28

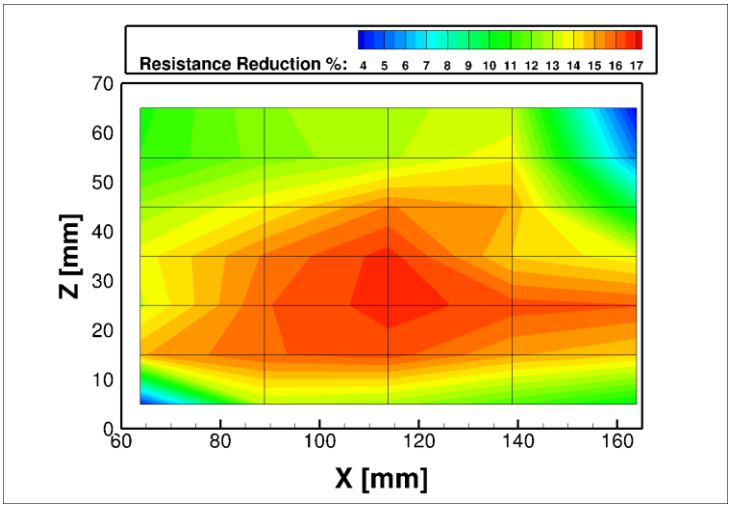

Figure 33. Visualization of gains with TPD for different positions. Bare hull.

The corresponding gains for the self-propelled case is presented in Table 6 and Figure 34. It would have been more interesting to present the reduction in delivered power, but that cannot be computed using the present approach with a body force disk representing the propeller. Presumably, the main contribution to the change in power will come from the resistance change. Changes in effective wake, propeller characteristics and relative rotative efficiency could probably be minimized by designing a new propeller for the TPD case.

It is seen that the optimum occurs at the same axial position, but at a smaller height (113,19). Also, the magnitudes of the gains are smaller. The maximum gain in the self-propelled case is 11.95%. From Figure 26 it also appears that the band of positive results is narrower.

Table 6. Computed resistance reduction with TPD for varying positions. Self-propelled hull

x [mm] / z [mm]	63	88	113	138	163
59	5.74	5.18	5.59	6.40	3.45
49	3.88	6.80	7.45	6.86	6.74
39	4.66	7.48	8.07	8.26	10.00
29	5.50	8.54	10.71	11.49	10.80
19	8.88	10.18	11.95	11.70	11.02
9	10.31	11.67	11.55	9.78	8.20
5	10.15	10.96	10.37	9.00	5.84

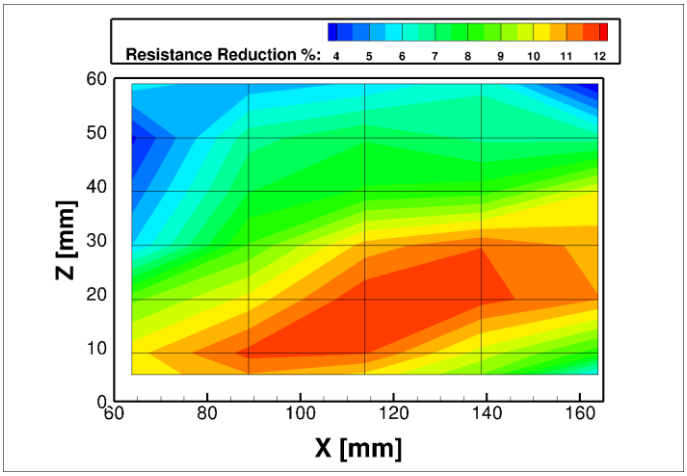

Figure 34. Visualization of resistance reduction with TPD for varying positions. Self-propelled hull.

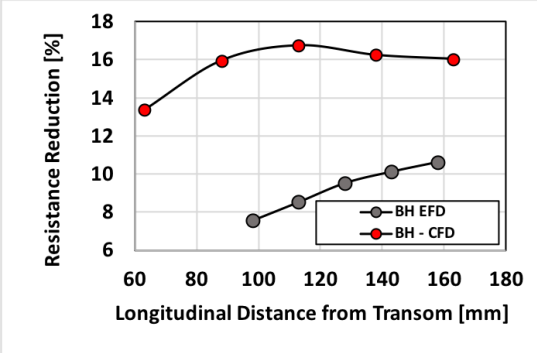

Figure 35. Comparison between computed and measured resistance reductions

A comparison between computed and measured resistance reductions for the bare hull is shown in Figure 35. The correspondence is not very good. While the maximum gain from CFD, as seen above, is about 17% it is only about 11% in the measurements. The optimum position is also different and considerably further aft in EFD. We have not been able to pinpoint the reasons for the differences, so far.

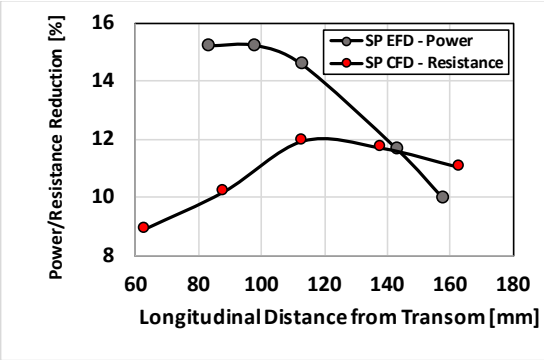

Figure 36. Computed reduction in resistance compared with measured reduction in power

Figure 36 shows the computed resistance reduction in self-propulsion and the measured reduction in power. Unfortunately, we cannot compare the same quantities, since the resistance (thrust) could not be measured, only the moment and rpm, from which the power could be computed. Again, there is a significant difference between CFD and EFD. Now the gain is larger in the experiments, more than 15% at the optimum position.

Figure 37 is the last one in this section. It shows the gain in self-propulsion versus Froude number for the optimum positions of the TPD. Somewhat surprisingly, the gain increases when the Froude number is reduced. For EFD the largest gain in power is about 25% at Fn = 0.2. In the range Fn = 0.3 - 0.5 the gains are between 13 and 18 %, which is much more than anticipated. In the same range CFD varies between 9 and 16%. So, in both cases the reductions are considerable.

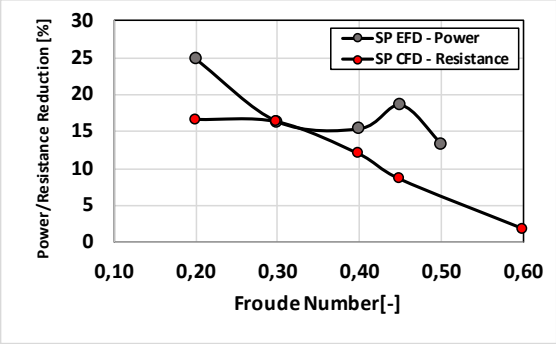

Figure 37. Measured and computed gains vs. Froude number

5.4 Other propulsion systems

In this section the performance of TPD is studies in presence of two propeller in comparison to its performance with one propeller. Moreover, possibility of employing TPD with waterjet propulsion is also studied.

5.4.1 Effect of two propellers

In the previous self-propulsion simulations only one centered propeller has been employed in the simulation. However, in this section, two propellers are used to carry out the self-propulsion simulations. The objective is to study the dependency of the TPD performance on a different arrangement of the propulsion system. As stated in the computational method description section, a body-force model has been employed to model the propeller effect. The dark blue areas in Figure 38 show the regions where the body-force has been deployed to accelerate the

flow. In case of one propeller, the propeller center is placed on the hull symmetry plane (diameter = 100 mm). In this section, two propellers of smaller diameters are used (diameter = 70 mm) which are placed 150 mm away from the hull symmetry, in the transvers direction (Figure 38).

Table 7 shows the results obtained from CFD self-propulsion simulations in presence of one-propeller as well as two-propellers, with and without TPD. The optimum TPD position obtained from self-propulsion systematic optimization is used for all these simulations. If we compare only the self-propelled hulls without TPD, we notice that the hull resistance (propeller thrust) has increased by about 1.5 N when two propellers are used. Since the sinkage and trim angles for these hulls are almost the same, only the local flow changes are contributing to the increased hull resistance. The main cause is the decreased wetted area of the transom with two propellers in comparison to the self-propulsion simulation with one propeller. As a result, the transom pushing force for the hull with two propellers decreases (about 1.3 N) which almost contributed to the entire difference between the transom pushing force difference between the hull with one propeller and two propellers.

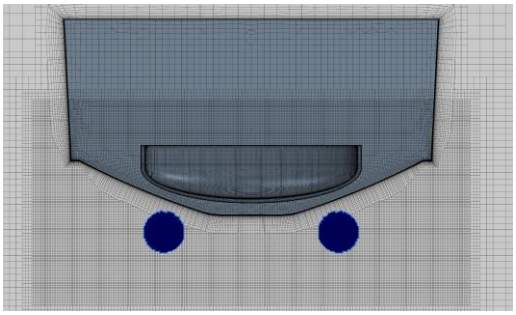

Figure 38. Body force application region for two propellers.

From the systematic TPD position optimization study in self-propulsion we know that the TPD reduces the self-propelled hull resistance (thrust) by 11.95%. The resistance reduction increases to 14.42% when two propellers are used. The sinkage and trim of these hulls are the same, and again the local flow changes must be responsible for the lower resistance of the hull with two propellers. Actually, the pushing force of TPD is slightly smaller for the hull with two propellers (0.6 N in comparison to 1.2 N). However, due to the interaction between TPD and the transom, the wetted surface area of the transom becomes the same for both of the hulls. Remember that the transom wetted surface area without TPD was smaller for the hull with two propellers. In presence of TPD the hulls have exactly the same wetted surface area and thus the transom pushing force. Thus, the transom pushing force (increased wetted surface area) is the main reason for the lower net resistance of the hull with two propellers.

Table 7. Variation of hull aft draft, trim and resistance for BH: bare hull, SP: self-propulsion with 1 and 2 propellers with and without TPD.

	Aft draft [mm]	Trim [degrees]	Resistance [N]	Resistance Reduction [%]
BH	-16.9	0.49	34.04	-------
SP: 1 Propeller	-19.3	0.61	32.21	-------
SP: 1 Propeller + TPD	-14.9	0.39	28.36	11.95
SP: 2 Propellers	-19.6	0.60	33.77	-------
SP: 2 Propellers + TPD	-14.8	0.39	28.90	14.42

These results confirm that TPD performs slightly better if the hull has two smaller propellers instead one large.

5.4.2 TPD and waterjet propulsion

The TPD was also tested with waterjet propulsion, as seen in Figure 39. For this case a hole is needed in the TPD, which reduces its effect. Moreover, the jet entrains the recirculating water, so its momentum in the forward direction is reduced. Therefore a smaller gain can be expected. There is also a practical problem with this setup, since in reality there is normally a gear for directing the jet behind the nozzle. This gear would interfere with the TPD, and more importantly, the jet will not hit the hole in the TPD when the jet is deflected.

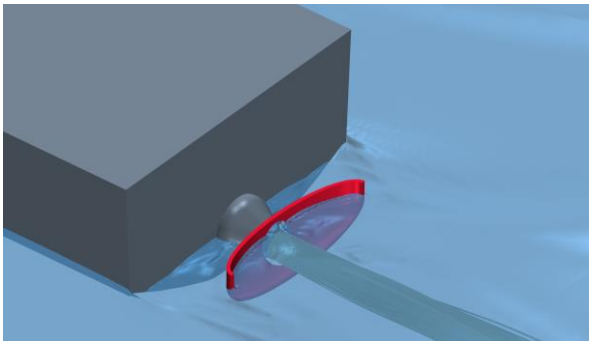

Figure 39. Application of TPD for a waterjet propelled hull.

Table 8 shows an analysis of the force components in waterjet propulsion for two Froude numbers without (WJ) and with (WJTP) the TPD. At the lower Froude number the TPD contributes 3.52 N to the pushing force, but the transom force is reduced from 12.46 to 9.86 N. Together there is a pushing force of 0.92 N. The total positive effect is 1.56 N (4.29%), where the remaining part must come from a reduction in the hull resistance due to less sinkage and trim.

At the higher Froude number the TPD force is smaller (2.18 N) and the reduction in transom push is smaller as well (from 5.44 to 4.08 N). The net effect is about the same as before. 0.82 N, but very surprisingly there is an increase in the total resistance, so the total effect is negative, -2.72%! This effect needs to be more investigared.

Table 8. Force components on TPD, transom and hull with waterjet propulsion at two different speeds

	Fn	Hull	TPD Concave Side	PD Convex Side	PD Total	Transom	PD + Transom	Total	Resistance Reduction%
WJ	0.3	48.86	0	0	0	-12.46	-12.46	36.4	-
WJPD	0.3	48.22	-6.02	2.5	-3.52	-9.86	-13.38	34.84	4.29
WJ	0.4	92.28	0	0	0	-5.44	-5.44	86.84	-
WJPD	0.4	95.46	-4.02	1.84	-2.18	-4.08	-6.26	89.2	-2.72

In Figure 40 the water level on both sides of the TPD is presented with the hole for the waterjet in the middle. This figure should be compared with Figure 26 for the towed case. Figure 41 shows the corresponding pressure distributions and should be compared with Figure 27. Apparently, the hole and the action of the jet changes the water level and pressure considerably.

Figure 40. Wetted surface area of TPD used in waterjet. (left) concave side and (right) convex side of TPD.

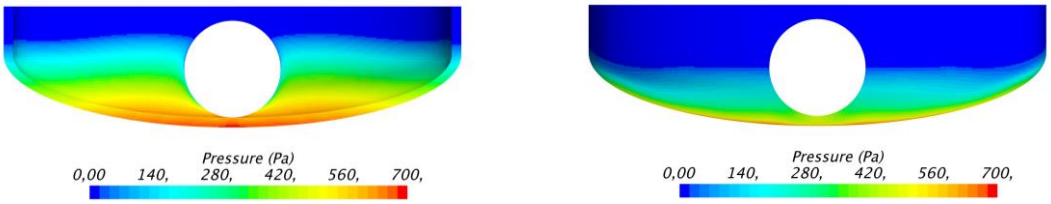

Figure 41. Pressure distribution on TPD. (left) concave side and (right) convex side of TPD.

6 Conclusions

Based on the numerical and experimental studies a number of conclusions may be drawn:

- A spoon shaped TPD is considerably more efficient than a flat one. Rectangular and triangular plates were investigated but both were inferior to the newly developed spoon shape.

- For the optimum position of the TPD the main effect of the TPD is, as expected, the pushing force generated by the device when it is located in the recirculating flow. There is also a positive effect of a water level rise at the transom, but that is much smaller. The effect on sinkage and trim is minor.

- For other positions of the TPD, particularly in the vertical direction, the role of the TPD changes. For a too low position the pushing force is reduced considerably and may even become negative. This effect is however compensated to some degree by an increase in the water level on the transom and a smaller trim of the hull.

- The waves are reduced by the TPD behind the hull, but this effect seems to diminish in the far wake

- A global momentum analysis showed that there is an increase in pressure in the wake, while the total momentum change is small. The total head is thus larger in the wake due to the smaller resistance with the TPD.

- Systematic variations in position for the towed case showed a maximum resistance reduction in CFD by 17%, while the measured maximum gain in EFD was 12%. This is for the most interesting Froude number, Fn = 0.40

- For the self-propelled case the maximum resistance (thrust) reduction was 12% in CFD, while the reduction in power for EFD was 15%, again at Fn = 0.4

- Both CFD and EFD indicate increasing gains for lower Froude numbers, but it should be kept in mind that the large transom is a great disadvantage at these low speeds.

- For higher Froude numbers there is a reduction in gain, but CFD indicates that there is still a small gain at Fn = 0.6. The highest Froude number in EFD was 0.5 and the reduction in gain was small compared to Fn = 0.4.

- CFD results for two propellers indicate that larger gains may be obtained if the thrust is distributed to two propellers rather than one.

- TPD:s are not suitable for waterjet propulsion. There are large practical difficulties with the setup and the gains are much smaller, even negative in some cases

7 Acknowledgement

The support from Trafikverket through the grant FUD 6482, 2018 is gratefully acknowledged.